Niobium films produced by magnetron sputtering using an Ar-He mixture as discharge gas

G.-M. Schucan (*ETH Zürich, 8093 Zürich, Switzerland)*
C. Benvenuti, S. Calatroni (*CERN, 1211 Geneva 23, Switzerland)*

Abstract

Superconducting RF accelerating cavities have been produced at CERN by sputter-coating, with a thin niobium layer, cavities made of copper. In the present work, the discharge behaviour and niobium film properties have been investigated when part of the argon sputtering gas is replaced with helium. Helium is chosen because of its low mass, which reduces the energy lost by the niobium atoms colliding with the sputter gas atoms. The higher niobium atom energy should lead to higher adatom mobility on the substrate and, hence, to a larger grain size, a feature which is highly desirable to reduce the cavity surface resistance. It has been found that helium addition effectively helps to maintain the discharge at considerably lower argon pressures, via metastable-neutral ionisation and high secondary electron yield. However, a large amount of helium is trapped in the film, amount which is proportional to the helium partial pressure during the discharge, resulting in a reduction of both Residual Resistivity Ratio and grain size.

1. Introduction

Superconducting RF accelerating cavities play a crucial role in present day accelerator technology. Whereas these cavities are traditionally made of niobium sheet, for the upgrade of the Large Electron Positron Collider (LEP) at CERN, copper cavities internally coated with a 1.5 µm thick niobium layer will be used [1]. These cavities, currently being produced by industry [2], are coated by means of a cylindrical magnetron sputtering system, with pure Ar as the process gas [3].

As a result of the work carried out so far [4], the following guidelines for the optimisation of the polycrystalline Nb film with respect to RF performance were tentatively established:

- crystal grain size should be as large as possible
- grain boundaries should be as clean as possible
- the intragrain Residual Resistivity Ratio (RRR), i.e. the ratio of resistivities at 300 K and 10 K, should be around 15, where the RF surface resistance presents a minimum

Experiments at CERN have shown that the RRR, as well as the grain size, increases with increasing coating temperature [5]. Tests on Nb-coated copper samples yielded RRR values as high as 40 and an average grain size of up to 0.2 µm on the surface for a substrate temperature of 550°C, compared to RRR values of about 20 and a grain size of up to 0.1 µm at the standard temperature of 200°C. However, to avoid the risk of cavity collapse due to copper annealing, the cavity cannot be heated above 200°C.

It was also found that high discharge power and low Ar pressure during the discharge lead to optimum film quality. Actually, a higher discharge power increases the flux of sputtered atoms impinging on the film, while a reduction of the discharge pressure increases their energy. Both effects result in a higher surface temperature and, in turn, to higher mobility of the Nb atoms, i.e. to more favourable conditions for growing larger crystal grains.

For the present standard cavity coating procedure the discharge parameters are optimised within the limits of the given configuration. The maximum discharge power is limited by the heating of the cathode, whereas the discharge pressure cannot be reduced at will, because discharge instabilities start to occur below a certain threshold, eventually leading to discharge extinction if the pressure is reduced further.

An attempt has therefore been made to substitute part of the Ar process gas by He. Since He is much lighter than Ar, this reduces the energy loss of the Nb atoms by gas scattering and therefore increases their impinging energy.

He has a very low Nb sputtering yield (in the energy range considered about 0.02, compared to 0.5 for Ar [6]). However, He may participate in supporting the discharge by the following processes:

- asymmetric charge transfer

$$He^+ + Ar \rightarrow Ar^+ + He \qquad (1a)$$

- metastable-neutral ionisation

$$He^* + Ar \rightarrow He + Ar^+ + e^- \qquad (1b)$$

- higher secondary electron yield (1c)

where He^* stands for a metastable He atom. The reverse process of charge transfer (1a) is negligible because it is strongly endoergic and therefore has a low cross section compared with the other processes [7]. The reverse process of the metastable-neutral ionisation (1b) is unlikely to happen because it would require three particles to collide at once.

At a certain He partial pressure the processes (1a-1c) may help in keeping the same sputtering rate in spite of a lower Ar partial pressure. The mean free paths associated with charge transfer (λ_c) and with metastable-neutral ionisation (λ_{mn}) are given by

$$\lambda_c = 1/\sigma_c n_{Ar} \qquad (2)$$
$$\lambda_{mn} = 1/\sigma_{mn} n_{Ar}$$

where σ_c (=$2.7\cdot10^{-16}$ cm^2), σ_{mn} (=$7.6\cdot10^{-16}$ cm^2) [6] are the respective cross sections and n_{Ar} is the Ar atom density.

The Ar pressure in the standard coating procedure is $8\cdot10^{-4}$ mbar. If this pressure is reduced to 60%, λ_c becomes about 1.3 m, so that charge transfer will be negligible for a cavity where the distance between the cathode and the substrate is about 30 cm. On the other hand, the metastable-neutral ionisation mean free path λ_{mn} becomes about 40 cm. Considering also that the lifetime of the

He 2^3S metastable is 10^{-4} sec [8], i.e. about six times longer than the time a 10 eV He^* needs to travel one λ_{mn}, the He^* has a considerable chance to relax by metastable-neutral ionisation.

In addition, the higher secondary electron yield of the He causes more electrons to be emitted from the cathode. These electrons in turn create Ar ions and therefore help to increase the total sputtering rate.

On the basis of these considerations, tests with different Ar-He gas mixtures were undertaken.

2. Experimental

Coating was performed in a cylindrical magnetron sputtering system as shown in Fig. 1 [1]. A 500 MHz stainless steel cavity, used instead of the usual copper cavity, allows the mounting of four sample holders and direct connection to a gas analyser. Each sample holder can expose six samples in turn. The cathode consists of a cylindrical stainless steel tube inserted along the cavity axis and linked tightly to the cavity through a ceramic insulator. This tube is surrounded by a high purity niobium liner (RRR=100), i.e. the actual sputtering source, and contains a solenoid electromagnet which provides the magnetic field required for the magnetron effect (~140 G at the cathode surface). The tube and the magnet are cooled by a constant flow of refrigerating fluid. During the discharge the magnet current is automatically controlled in order to keep the discharge current constant.

Pumping is achieved by a 170 l/s turbomolecular pumping station. After a 24 hours bake-out at 200°C an ultimate pressure in the low 10^{-9} mbar range is reached. Two bakeable injection lines, equipped with precision injection valves, allow the injection of a constant flow of Ar and He into the system during the discharge. Gas purity is better than 99.9999% for both gases. The He injection line is equipped with a liquid nitrogen cooled trap to further purify the injected gas. The gas composition is continuously monitored by a residual gas analyser differentially pumped by a second turbomolecular pumping station.

Standard coating parameters used in this system are the following:

- cathode voltage: U= - 400 V (with respect to ground)
- discharge current: I=7.5 A
- argon pressure: $p_{Ar}=8\cdot10^{-4}$ mbar
- coating temperature: T=200°C

This leads to a discharge power of 3 kW and to a film growth rate of about 4 Å/s.

For the coating with an Ar-He mixture as discharge gas two different approaches were followed. The first approach (in the following denoted by method 1) consisted in reducing the Ar pressure to a certain fraction of the standard value ($8\cdot10^{-4}$ mbar) and then adding He until the standard discharge conditions (U=-400 V, I_{dis}=7.5 A, I_{coil}=2.5 A) were reached. The amount of He needed to compensate for the reduction of the Ar pressure can be determined in this way. For the second approach (method 2) an Ar pressure of 60% of the standard pressure (i.e. $4.8\cdot10^{-4}$ mbar) was fixed and various quantities of He were added. The standard discharge power was then attained by adjusting the coil current and thus the magnetic field of the electromagnet. With this method the effect of the He on the film quality can be more easily deduced.

All the samples mentioned in this report are labelled according to their respective Ar and He pressures normalised to the standard Ar pressure of $8\cdot10^{-4}$ mbar (e.g. 0.6/0.2 denotes a sample made with an Ar pressure equal to 60% and a He pressure equal to 20% of the standard value, i.e. $p_{Ar}=4.8\cdot10^{-4}$ mbar and $p_{He}=1.6\cdot10^{-4}$mbar). This same notation is also used for the x-axis scale of all the graphs herein reported.

Using method 1, coatings at 0.9, 0.7, 0.5 and 0.3 times the standard Ar pressure were produced. Fig. 2 shows the resulting gas compositions required to obtain standard conditions and the corresponding sample labels. In addition, a standard 1.0 reference sample was grown. It is seen that more He is needed than just the missing Ar pressure.

Fig. 3 shows the He pressure scan performed according to method 2. For a fixed 0.6 Ar pressure, He pressures of 0.1, 0.2, 0.4, 0.8, 1.6 times the standard Ar pressure were chosen. In order to compensate for the decrease in discharge current, the coil current had to be increased. The adjustment is made automatically by simple electronic control.

In the first phase, films with a standard coating time (50 min) were produced on quartz substrates using all gas mixtures shown in Fig. 2 and 3, to determine the sputtering rate. In the second phase, films of various thickness were made according to method 2, both on copper and quartz substrates to determine the grain growth behaviour and the dependence of the RRR on film thickness and grain size. Films of standard thickness were also deposited according to method 2 on stainless steel ribbons for thermal outgassing measurements (see paragraph 3).

The measurement of film thickness was performed with a Stylus-Method Profilometer. RRR values were measured in a liquid He cryostat using a four-point method. Average crystal grain sizes were determined by X-ray diffraction. The thermal outgassing measurements were made in a UHV system, equipped with a gas analyser and thermocouples, where the sample may be heated resistively up to 1100°C. The evolution of the degassing species was continuously monitored while the Nb-coated stainless steel ribbons were heated with a temperature ramping of 5°C/min.

3. Results

The film thickness obtained within the standard coating time of 50 min are reported in Fig. 4 and 5. When applying method 1 (Fig. 4), the thickness decreases with decreasing Ar pressure in spite of the He addition. Fig. 5 shows that for films grown according to method 2 the thickness decreases only slightly when increasing the He pressure.

Table 1 and 2 show the RRR values and the crystal grain sizes of these samples. For both values an important degradation with increasing He pressure is observed.

Thermal outgassing measurements revealed He contamination of the film. Due to the start of sublimation of the stainless steel components, the temperature for these measurements was limited to 1100°C. At this temperature He outgassing is still present so that these measurements can only give a lower limit for the actual He content of the film. A rough estimate of the He pumping speed of the film, based on the He pressure reduction taking place when the discharge is ignited, allows to give an upper limit for this contamination. Both values are found to be proportional to the He pressure present during the coating as is shown in Fig. 6.

4. Discussion

The addition of He allows the Ar pressure to be considerably reduced without loosing the discharge stability. This shows the effectiveness of the metastable-neutral ionisation and of the higher secondary electron yield of He. The total sputtering rate was found to be only slightly reduced, even for large Ar pressure reductions.

On the other hand, adding He to Ar in the coating discharge leads to a clear deterioration of the RRR and to a reduction of Nb crystal grain size. A legitimate question to be asked is whether the lower film quality is a consequence of reducing the Ar pressure or of increasing the He pressure in the discharge.

In Fig. 7 and 8 the dependence of RRR and average grain size on the normalised He pressure is represented. It is evident that data from both methods are interchangeable. Since in method 1 the Ar pressure is progressively decreased and in method 2 it is kept constant, it may be concluded that the deterioration of film quality is not due to the Ar pressure reduction but rather to the increasing He pressure.

The correlation between the measured RRR values and the grain size in polycrystalline metal films is not yet fully understood. Various models have been proposed, [9, 10, 11, 12] which assume that an electron travelling through a polycrystalline metal undergoes scattering by defects and phonons, and, in addition, has only a certain transmission probability T to cross a grain boundary. It is clear that in this case the overall resistance increases as the number of grain boundaries increases.

If the RRR degradation found in this study is only due to the reduced average grain size D, then the ratio RRR/D should, to a first approximation, be constant. Fig. 9 shows that this is not the case. We can conclude that the RRR degradation must be produced, to a large extent, by impurity trapping in the film.

As discussed in ref. 5, it is a vital question for the RF behaviour of the film whether these impurities are uniformly distributed within the grain or whether they are accumulated at the grain boundaries. If He trapping occurs only inside the grains and the transmission coefficient is unchanged, its effect would be a reduction of the intragrain RRR of the film so that it could be used as a dopant to control the RRR. By this means the RF resistance could be reduced to its minimum. On the other hand, an increased impedance at grain boundaries would result in a much larger RF resistance.

For common gases dissolved in bulk metal, the variation of the resistivity as a function of the gas concentration is reported in the literature. For Nb this dependence is given in the form [13]:

$$\rho(x_A) = 14.4 + c_A \cdot x_A \ [\mu\Omega \cdot \text{cm}] \qquad (3)$$

where 14.4 $\mu\Omega\cdot$cm is the phononic contribution at 300 K, x_A is the atomic fraction (<0.03) of some gas A incorporated in the Nb, and c_A is a gas specific constant, independent of temperature, ranging from 65 for hydrogen to 450 for oxygen. The corresponding RRR is:

$$RRR = \frac{\rho(300\text{K})}{\rho(10\text{K})} = \frac{14.4 + c_A \cdot x_A}{c_A \cdot x_A}, \qquad (4)$$

assuming that the phononic contribution to the resistivity disappears at low temperature.

The effects of He on the resistivity of Nb are generally studied in the literature on samples produced by irradiation with He ions [14]. By re-examining these data we obtain a c_A of 70 for an atomic fraction up to about 0.01. The reported c_A value results from the scattering effects of both the defects created by the ion bombardment and the He inclusions, and therefore it may be considered pessimistic in the present case, where only the inclusion of He atoms takes place.

Assuming a "worst case" scenario, i.e. taking the upper impurity limit of Fig. 6 and this pessimistic value for c_A, we find that the RRR calculated with (4) is still higher than the measured value (see Fig. 10). This gives a clear indication that a substantial part of the RRR decrease is due to He accumulated at the grain boundaries. This conclusion is also supported by the observed reduction of crystal grain size. Residual gas adsorption has been reported to cause an adatom mobility reduction, which in turn hinders grain growth [15].

5. Conclusions

Experiments showed that in the pressure range considered the metastable-neutral ionisation and the higher secondary electron yield of He efficiently maintain the discharge at an only slightly reduced sputtering rate in spite of the very low sputtering yield of He. On the other hand, charge-transfer was found to be of negligible importance by theoretical considerations.

The analysis of the resulting films revealed that the benefit of the higher impinging energy of the Nb atoms on the substrate is largely offset by an important He trapping in the film, which is shown to be proportional to the He partial pressure during the discharge. This leads to a reduction of both RRR and grain size. This RRR reduction is attributed to a large decrease in transmission probability between crystal grains caused by He impurities accumulated at the grain boundaries, which is also believed to hinder grain growth.

These conclusions hold for Nb films produced by magnetron sputtering. Other materials could display more favourable behaviour with respect to He trapping. The proposed approach could then be particularly useful if diode sputtering is used. Diode sputtering makes use of higher pressures, and therefore metastable-neutral ionisation would be more efficient and charge transfer would provide non-negligible effects.

6. Acknowledgements

The authors are indebted to M. Hauer for technical assistance and M.P. Reinert for thermal outgassing measurements.

Tables

Table 1: Measured thickness, RRR and average grain size D for films produced according to method 1.

sample	*thickness [µm]*	*RRR*	*D [µm]*
1/0	1.50	18	0.096
0.9/0.1	1.45	14	0.089
0.7/0.5	1.40	10	0.078
0.5/2.6	1.30	4.5	0.045
0.3/6.5	1.20	3.2	0.035

Table 2: Measured thickness, RRR and average grain size D for films produced according to method 2.

sample	*thickness [µm]*	*RRR*	*D [µm]*
0.6/0.1	1.50	16	
0.6/0.2	1.50	11	0.107
0.6/0.4	1.45	9.2	0.079
0.6/0.8	1.40	8.1	
0.6/1.6	1.40	6.9	0.056

Figure Captions

Fig. 1: Schematic view of the cylindrical magnetron sputtering configuration for single-cell 500 MHz cavities.

Fig. 2: Gas compositions employed in experiments carried out according to method 1. The labels reported on the x-axis indicate the fractions of the standard Ar pressure adopted for the Ar and He partial pressures.

Fig. 3: Gas compositions employed in experiments carried out according to method 2.

Fig. 4: Thickness values measured on films produced according to method 1.

Fig. 5: Thickness values measured on films produced according to method 2.

Fig. 6: Lower and upper limit for He concentration. The upper limit is obtained from He film pumping evaluation, the lower limit from outgassing measurements.

Fig. 7: Variation of RRR as a function of He pressure for films produced according to method 1 and method 2.

Fig. 8: Variation of crystal grain size as a function of He pressure for films produced according to method 1 and method 2.

Fig. 9: Variation of the ratio RRR/grain size (D) as a function of He pressure.

Fig. 10: Comparison between the RRR reduction calculated according to eq. (4) ("worst-case" scenario) and measured on samples produced according to method 2.

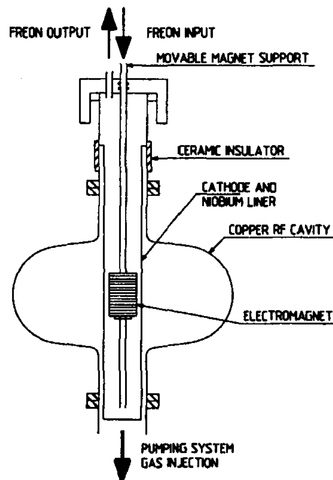

Fig. 1

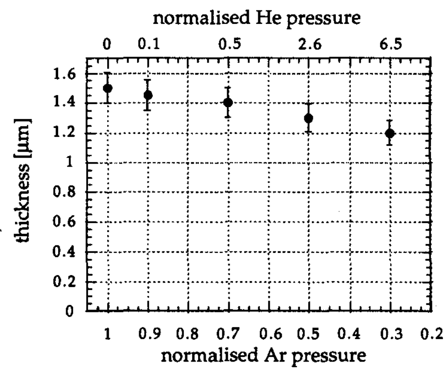

Fig. 4

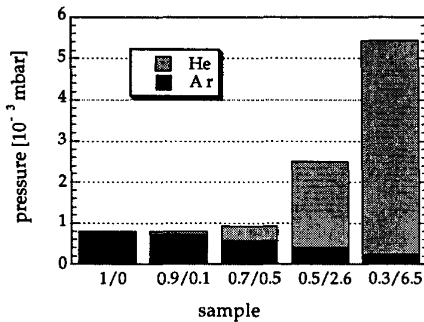

Fig. 2

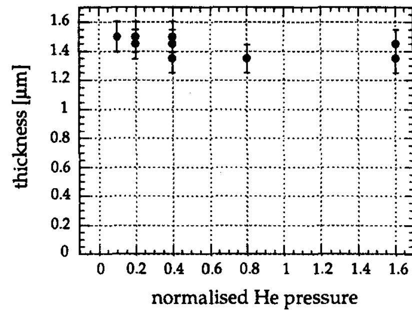

Fig. 5

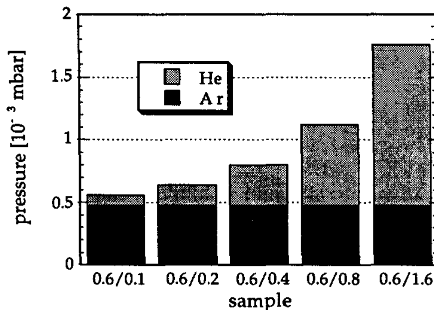

Fig. 3

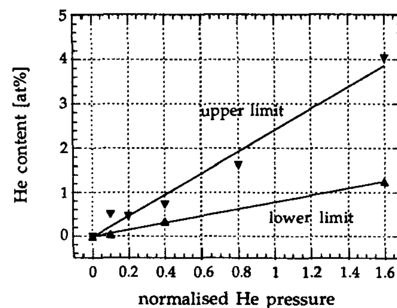

Fig. 6

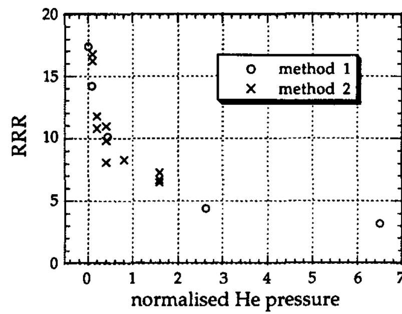

Fig. 7

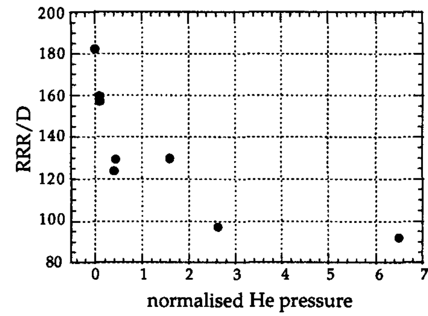

Fig. 9

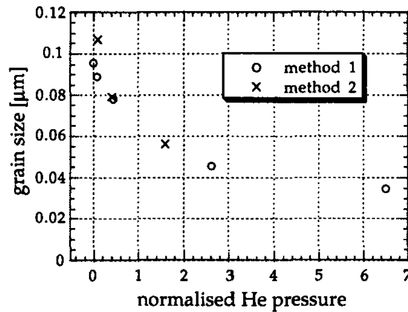

Fig. 8

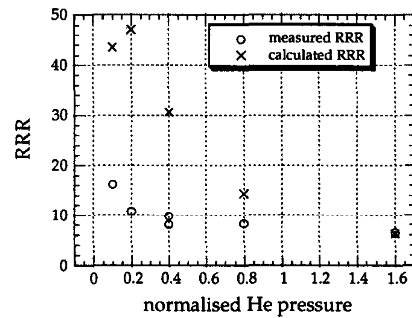

Fig. 10

References

[1] C. Wyss, Proc. of the EPAC 92 (Editions Frontières, Gif-sur-Yvette, 1992), pp. 400, 402.
[2] C. Benvenuti, S. Calatroni, E. Chiaveri, G. Orlandi and W. Weingarten, Cryogenics **34** ICEC Supplement, 57 (1994).
[3] C. Benvenuti, D. Bloess, E. Chiaveri, N. Hilleret, M. Minestrini and W. Weingarten, Proc. of the 3rd Workshop on RF Superconductivity (ANL, Argonne, 1988) pp. 445, 453.
[4] C. Benvenuti, S. Calatroni and G. Orlandi, Physica **B 197**, 72 (1994).
[5] G. Orlandi, C. Benvenuti, S. Calatroni and F. Scalambrin, Proc. of the 6th Workshop on RF Superconductivity (CEBAF, Newport News, 1993), pp. 718, 729.
[6] N. Matsunami, Y. Yamamura, Y. Itikawa, N. Itoh, Y. Kazumata, S. Miyagawa, K. Morita, R. Shimizu and H Tawara, Atomic Data and Nuclear Data Tables **31**, 1 (1984).
[7] Z. Donkó, K. Rósza and M. Jánossy, J. Phys. D: Appl. Phys. **24**, 1322 (1991).
[8] F. K. Kneubühl and M. W. Siegrist, *Laser*, 3rd ed. (Teubner, Stuttgart, 1991), p. 242.
[9] K. Fuchs, Proc. Camb. Phil. Soc. **38**, 100 (1938).
[10] A. F. Mayadas and M. Shatzkes, Phys. Rev. **B 4**, 1382 (1979).
[11] G. Reiss, J. Vancea and H. Hoffmann, Phys. Rev. Lett. **19**, 2100 (1986).
[12] A. Knäbchen, J. Phys: Condens. Matter **3**, 6989 (1991).
[13] G. Hörz, H. Speck, E. Fromm and H. Jehn, *Gases and Carbon in Metals, Pt. VII (2)*, (Fachinformationszentrum, Eggenstein-Leopoldshafen, 1981), pp. 4, 34
[14] M. P. Volkov, Yu. N. Sokurskiy, S. I. Tsypkin, V. I. Chuyev and V. N. Shishov, Phys. Met. Metall. **59**, 6, 58 (1985)
[15] J. A. Thornton, J. Vac. Sci. Technol. **4**, 666 (1974).